


Constrained Amorphous Interphase in Poly(L-lactic acid): Estimation of the Tensile Elastic Modulus

Laura Aliotta, Massimo Gazzano, Andrea Lazzeri,* and Maria Cristina Righetti*


 Cite This: *ACS Omega* 2020, 5, 20890–20902

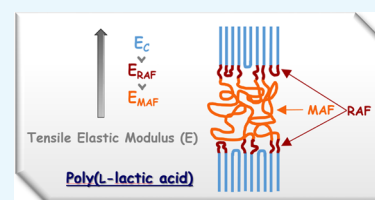

Read Online

ACCESS |

 Metrics & More

 Article Recommendations

ABSTRACT: The mechanical properties of semicrystalline PLLA containing exclusively α' - or α -crystals have been investigated. The connection between experimental elastic moduli and phase composition has been analyzed as a function of the polymorphic crystalline form. For a complete interpretation of the mechanical properties, the contribution of the crystalline regions and the constrained amorphous interphase or rigid amorphous fraction (RAF) has been quantified by a three-phase mechanical model. The mathematical approach allowed the simultaneous quantification of the elastic moduli of (i) the α' - and α -phases (11.2 and 14.8 GPa, respectively, in excellent agreement with experimental and theoretical data reported in the literature) and (ii) the rigid amorphous fractions linked to the α' - and α -forms (5.4 and 6.1 GPa, respectively). In parallel, the densities of the RAF connected with α' - and α -crystals have been measured (1.17 and 1.11 g/cm³, respectively). The slightly higher value of the elastic modulus of the RAF connected to the α -crystals and its lower density have been associated to a stronger chain coupling at the amorphous/crystal interface. Thus, the elastic moduli at T_{room} of the crystalline (E_C), mobile amorphous (E_{MAF}), and rigid amorphous (E_{RAF}) fractions of PLLA turned out to be quantitatively in the order of $E_{\text{MAF}} < E_{\text{RAF}} < E_C$, with the experimental E_{MAF} value equal to 3.6 GPa. These findings can allow a better tailoring of the properties of PLLA materials in relation to specific applications.



1. INTRODUCTION

The growing request of “green” chemicals and processes has progressively increased the interest toward the application of more environmentally friendly polymeric materials. Bio-based and biodegradable polymers have become the topic of many investigations by both academia and industry. Poly(lactic acid) (PLA) is one of the bio-based and biodegradable polymers most studied because it is widely present on the market, especially for biomedical and packaging purposes. In addition to its biodegradability and renewability, PLA exhibits stiffness and strength comparable to those of traditional petroleum-based polymers, with an elastic modulus of about 3–4 GPa and a tensile strength in the range of 40–60 MPa.¹ On the other hand, drawbacks for its utilization are a high cost with respect to traditional petroleum-derived polymers and a low toughness, which makes it a brittle polymer. A maximum elongation at break of around 4% strongly limits its applications when fracture toughness and high ductility are required. Nevertheless, the mechanical properties of PLA remain very attractive¹ and can be modulated as a function of (i) L- and D-lactic acid unit content and, consequently, (ii) the morphology and crystal structure. It is well known that the term PLA designates a variety of polymers containing different sequences and ratios of L- and D-units, whereas PLLA or PDLA refer to the homopolymers or copolymers containing a very small amount of D-units or L-units, respectively. The effects of the enantiomeric L- and D-units on the thermal properties of PLA have been extensively studied.² With respect to PLLA, an

increase in the percentage of D-lactic acid units produces a decrease in the crystallization rate, crystallinity degree, and melting temperature due to the exclusion of D-units from the PLLA crystals. PLA copolymers containing more than 10–15% of randomly distributed D-units are totally amorphous and noncrystallizable.³ As the majority of the bacteria utilized for fermentation produce L-lactic acid, PLLA is a product that is commercially very important. For this reason, PLLA is the polymer investigated in the present study.

PLLA exhibits polymorphism as a function of the crystallization conditions under normal industrial processing conditions (i.e., injection molding and extrusion).⁴ The α -form, the most stable polymorph characterized by two left-handed antiparallel 10₃ helical conformations packed in an orthorhombic cell, grows during melt and cold crystallizations at temperatures higher than 110 °C. At temperatures lower than about 100 °C, the growth of a slightly distorted and disordered form, the α' -form, is observed. This modification is characterized by a chain conformation more disordered with respect to the α -form, loose 10₃ helical packing, and slightly

Received: May 18, 2020

Accepted: June 23, 2020

Published: August 13, 2020



larger unit cell dimensions with respect to the α -form.^{5,6} In the intermediate T_c range between 100 and 110 °C, both α' - and α -forms grow under normal processing conditions, with the percentage of α -form increasing with T_c .^{6–9} The conformationally disordered α' -modification is metastable below 150 °C, and it converts irreversibly into the α -form around 160 °C upon heating at rates that are typically applied in conventional DSC.^{10,11} Additional crystal polymorphic forms, as the trigonal β -form, which develops upon stretching the α -phase at elevated temperature, and the orthorhombic γ -form, which grows on hexamethylbenzene substrates, are not interesting from an industrial point of view.⁴

Semicrystalline PLLA exhibits also different amorphous fractions, which, due to their various distances from the crystalline regions, are characterized by dissimilar mobility.¹² Besides a mobile amorphous fraction (MAF), which vitrifies/devitrifies in the glass transition (T_g) region, in PLLA, there exists also a constrained or rigid amorphous fraction (RAF) located at the crystal/amorphous interface. This interphase, found in almost all semicrystalline polymers,¹³ presents nanometric dimensions and reduced mobility due to the coupling with the close crystalline regions. This implicates that its vitrification/devitrification temperature is higher than T_g . The percentage of RAF in semicrystalline polymers depends not only on the crystallization conditions but also on the complete thermal history of the material.¹⁴ For PLLA, the rigid amorphous fraction was found to develop in parallel to the crystalline phase at low crystallization temperatures, whereas at higher temperatures, RAF formation was not observed or detected only during the final stages of the crystallization process.^{14,15}

A detailed description of the semicrystalline polymers, as composed of three different fractions, crystalline, mobile amorphous, and rigid amorphous fractions, is crucial for a full comprehension of the structure and properties of these materials because many macroscopic properties, as for example, mechanical and gas permeability properties, depend on their micro- and nanostructures. Thus, the physical properties of semicrystalline polymers can be interpreted correctly by taking into account not only the crystal phase and mobile amorphous fraction but also the RAF contribution.

Mechanical properties of semicrystalline polymers strongly depend on the polymorphic crystalline structure.^{16,17} For PLLA, the different regularity of chain conformation and packing along with different lattice dimensions influences the mechanical properties of the α - and α' -crystals.¹⁸ Experimental and theoretical evaluation of the ultimate elastic modulus of the α - and α' -forms of PLLA led to values slightly higher for the α -form (13.8 and 14.7 GPa, respectively) with respect to the α' -modification (12.6 and 12.9 GPa, respectively).¹⁸ This difference was found to reflect also on the elastic moduli of semicrystalline PLLA bulk samples.¹⁸

On the other hand, as regard to the rigid amorphous fraction, several investigations on different semicrystalline polymers have reported experimental evidence that the elastic modulus of the RAF could be close to that of the crystal phase.^{19–23} For polyethylene, theoretical estimations of the mechanical properties of the RAF, performed by Monte Carlo simulation²⁴ and micromechanical modeling,^{25,26} showed that the modulus of the rigid noncrystalline interlamellar phase is intermediate between those of the crystalline and amorphous bulk phases, thus attesting that the interphase plays an important role on the stress transfer between the crystalline

and mobile amorphous phases. For poly(ethylene terephthalate), micromechanical modeling demonstrated that the interphase stiffness is approximately 1.6 times the modulus of the amorphous phase.²⁷

All the mechanical models used to predict the properties of fiber-reinforced composites (for example, Kerner, Hashin–Shtrikman, Hirsch, Coran, Paul, Cox, etc., treatments),²⁸ can in principle be adapted to semicrystalline polymers because semicrystalline polymers can be considered mechanically similar to composites if the crystalline regions are assumed as a dispersed phase within the amorphous matrix.²⁹

The simplest mechanical models to estimate the elastic modulus (E) of a semicrystalline polymer, considered as a two-phase material, are given by the “parallel” and “series” models, which suppose parallel and series arrangements of the crystalline and amorphous phases. For the parallel arrangement, a uniform strain is assumed, whereas a uniform stress is presumed for the series arrangement.²⁸ For the parallel model, $E = V_C \cdot E_C + V_A \cdot E_A$, whereas for the series model, $1/E = V_C/E_C + V_A/E_A$, where E_C and E_A are the elastic moduli of crystalline and amorphous phases, and V_C and V_A are the corresponding volume fractions. These two simple models represent the upper and lower bounds of the tensile modulus predictions.

A more complex approach was provided by the two-phase Takayanagi model.^{30,31} This model relates a semicrystalline material to a combination of series and parallel elements (parallel model and series model) to take into account the different deformation that the crystalline and amorphous phases undergo under stress. The classical Takayanagi model has been widely applied to the prediction of the elastic modulus of semicrystalline polymers^{32–35} but also, as it is a two-phase approach, of polymeric blends,^{36,37} copolymers,³⁸ and composites^{39,40} due to its relatively simple analytical form.

Despite its extensive utilization, the original two-phase Takayanagi model is not able to describe in detail the mechanical behavior of semicrystalline polymers because it does not take into account the amorphous/crystal interphase, which exhibits organization and mobility markedly different from the bulk amorphous phase and moreover can be present in a high percentage.^{14,15} The same drawback has been reported, for example, if the model is applied to nanocomposites.^{41,42} In the case of filler percolation or in the presence of strong interactions between the nanofillers and the polymeric matrix, the introduction in the model of a third component became necessary. Examples of extension of the classical Takayanagi model to a three-phase system, to take into account the agglomerated fillers or the interfacial region in polymer nanocomposites, can be found in the literature.^{41,42}

Recently, a modified three-phase Takayanagi mechanical model has been utilized to quantify the elastic moduli at T_{room} of the crystalline (E_C), mobile amorphous (E_{MAF}), and rigid amorphous (E_{RAF}) fractions of poly(3-hydroxybutyrate-co-3-hydroxyvalerate) copolymers.⁴³ The mathematical resolution of the model allowed the direct determination of the moduli of the three fractions, which turned out to be quantitatively in the order of $E_{MAF} < E_{RAF} < E_C$, in perfect agreement with experimental and theoretical expectations.

Also in the present study, for the first time, the elastic modulus of the rigid amorphous fraction of PLLA is theoretically estimated by means of a three-phase Takayanagi model. To characterize separately the rigid amorphous fraction linked to α' - and α -crystals, PLLA was isothermally crystallized at two different temperatures, 95 and 110 °C, respectively, to

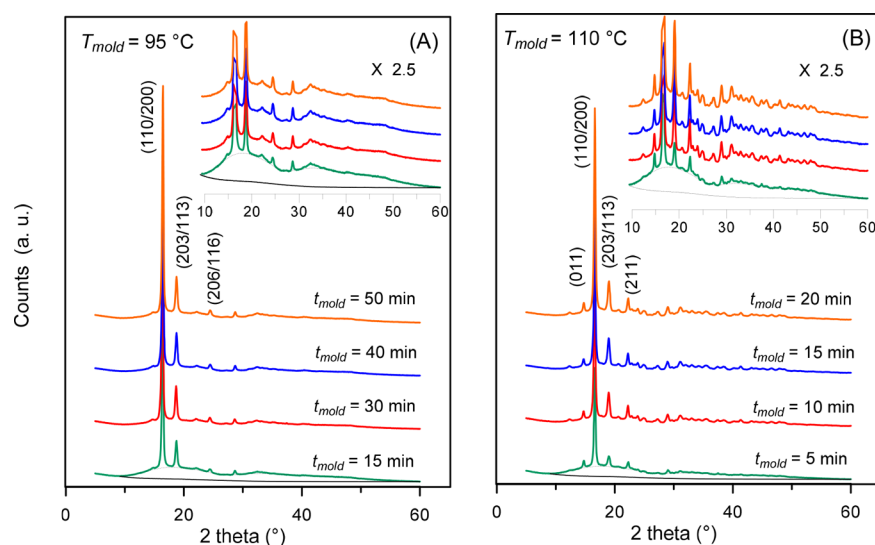


Figure 1. XRD patterns of PLLA after crystallization at $T_{\text{mold}} =$ (A) 95 °C and (B) 110 °C for the indicated molding times (t_{mold}). For the conditions $T_{\text{mold}} = 95$ °C, $t_{\text{mold}} = 15$ min, and $T_{\text{mold}} = 110$ °C, and $t_{\text{mold}} = 5$ min, the scattering of the amorphous fraction (black dashed lines) and the background (black solid line) are also shown. The insets are enlargements of the patterns.

prepare semicrystalline PLLA containing exclusively either α' - or α -crystals. As the application of the model allows the simultaneous quantification of the elastic moduli of the rigid amorphous fraction and crystalline fraction, the comparison of the calculated E_C 's with the corresponding experimental and theoretical values, reported in the literature for the α' - and α -crystals, can constitute a proof of the validity and reliability of the derived E_{RAF} data.

2. RESULTS AND DISCUSSION

2.1. XRD Analysis of PLLA after Different Crystallization Times at $T_{\text{mold}} = 95$ and 110 °C. Figure 1 shows the XRD patterns of PLLA at T_{room} after crystallization at the molding temperatures (T_{mold} 's) of 95 and 110 °C for different molding times (t_{mold}). All the patterns display features of semicrystalline specimens, with several peaks overlapped to a broad bell-shaped background. The crystalline phase of the samples prepared at $T_{\text{mold}} = 110$ °C belongs uniquely to the α -phase. It can be easily identified by the position of the most intense (110/200) and (203/113) peaks at the 2θ scattering angles of 16.6° and 19.0° and by the (011) and (211) peaks at 14.7° and 22.3°, respectively, as well as for several other less intense reflections at higher angles.^{5,7} Samples prepared at $T_{\text{mold}} = 95$ °C show uniquely the pattern of the α' -phase: the positions of the most intense (110/200) and (203/113) peaks are shifted at 16.5° and 18.8°, respectively, and in addition, the presence of a peculiar (206/116) peak at 24.5° is well evident; no peaks ascribable to the α -phase are present. It can be concluded that, exclusively, α' - and α -phases grow during crystallization at $T_{\text{mold}} = 95$ and 110 °C, respectively.

From the position of the most intense peaks, the mean crystallographic parameters were derived for the α' - and α -phases, as reported in Table 1. These values are very close to literature data.^{5,7} From the unit cell parameters, the density values of 1.245 and 1.265 g/cm³ were calculated for the totally crystalline α' - and α -phases of PLLA, respectively, in excellent agreement with literature data.¹⁸ The crystal fraction (X_C) values, calculated for all the specimens from the entire XRD profiles, are listed in Table 2 and discussed in the following section.

Table 1. Unit Cell Parameters of PLLA α' - and α -Crystals

crystal	a (Å)	b (Å)	c (Å)	V (Å) ³
PLLA α' -phase	10.74 ± 0.04	6.15 ± 0.03	29.10 ± 0.07	1922 ± 21
PLLA α -phase	10.70 ± 0.03	6.14 ± 0.02	28.82 ± 0.06	1893 ± 15

2.2. Thermal Characterization of Amorphous PLLA and after Different Crystallization Times at $T_{\text{mold}} = 95$ and 110 °C. Figure 2 shows the $c_{\text{p,app}}$ and $c_{\text{p,rev}}$ curves of the amorphous PLLA. The glass transition temperature (T_g), which is overlapped by a small enthalpy recovery peak connected to the structural relaxation occurred during the storage of 3 days at T_{room} after preparation, is centered around 56 °C, in agreement with literature data.⁴⁴ The specific heat capacity increment at T_g confirms that the specimen is completely amorphous.

It is worth noting that the glass transition in the $c_{\text{p,rev}}$ curve is observed at temperatures slightly higher with respect to the $c_{\text{p,app}}$ curves. This behavior can be explained considering that the apparent specific heat capacity represents the devitrification process that takes place at T_g upon linear heating rate, whereas the reversing heat capacity defines the “dynamic” glass transition, which is observed when the experimental timescale is close to the relaxation time of the amorphous segments.⁴⁵ For this reason, the dynamic glass transition is a function of the modulation period, shifting to higher temperatures with increasing modulation frequency.⁴⁵ In a TMDSC experiment, devitrification is a process characterized by a longer timescale with respect to the dynamic glass transition because many modulations occur during the glass transition.⁴⁶ Thus, an experiment performed with conventional linear heating rate could correspond to a TMDSC scan with low modulation frequency, with the result that the glass transition observed in the $c_{\text{p,app}}$ curves occurs at lower temperatures with respect to typical $c_{\text{p,rev}}$ curves.^{47,48}

Between approximately 75 and 110 °C, the $c_{\text{p,app}}$ curves exhibit an intense cold crystallization process, which as expected, is centered at increasing temperature with increasing heating rate. In correspondence with the cold crystallization

Table 2. Glass Transition Temperatures (T_g), Crystal Fraction (X_C), Mobile Amorphous Weight Fraction (X_{MAF}), Rigid Amorphous Weight Fraction (X_{RAF}), Experimental Elastic Modulus (E), Tensile Strength at Break (TS), and Elongation at Break Measured at T_{room} for PLLA after Crystallization at $T_{mold} = 95$ and 110 °C for Different Molding Times

condition	T_g (°C) ^a	X_C ^b	X_{MAF} ^b	X_{RAF} ^c	E (GPa)	TS (MPa)	elongation at break (%)
amorphous	57.0	0.00	1.00	0.00	3.60 ± 0.19	60.3 ± 2.2	3.60 ± 0.50
$T_{mold} = 95$ °C, $t_{mold} = 15$ min	59.0	0.29	0.48	0.23	3.86 ± 0.18	58.6 ± 1.2	1.68 ± 0.10
$T_{mold} = 95$ °C, $t_{mold} = 30$ min	63.5	0.38	0.39	0.23	3.83 ± 0.14	57.8 ± 1.1	1.68 ± 0.10
$T_{mold} = 95$ °C, $t_{mold} = 40$ min	64.5	0.39	0.38	0.23	3.82 ± 0.20	57.9 ± 2.7	1.67 ± 0.10
$T_{mold} = 95$ °C, $t_{mold} = 50$ min	65.0	0.40	0.36	0.24	3.92 ± 0.17	54.6 ± 1.7	1.60 ± 0.10
$T_{mold} = 110$ °C, $t_{mold} = 5$ min	58.0	0.18	0.75	0.07	3.95 ± 0.22	50.8 ± 3.0	1.37 ± 0.10
$T_{mold} = 110$ °C, $t_{mold} = 10$ min	60.0	0.38	0.47	0.15	4.08 ± 0.22	50.8 ± 3.2	1.36 ± 0.17
$T_{mold} = 110$ °C, $t_{mold} = 15$ min	61.0	0.40	0.42	0.18	4.19 ± 0.19	50.6 ± 2.5	1.31 ± 0.15
$T_{mold} = 110$ °C, $t_{mold} = 20$ min	62.0	0.42	0.38	0.20	4.42 ± 0.10	49.7 ± 3.0	1.24 ± 0.24

^aEstimated error from repeated measurements: ±0.5 K. ^bEstimated error from repeated measurements: ±0.02. ^cEstimated errors from repeated measurements: ±0.04.

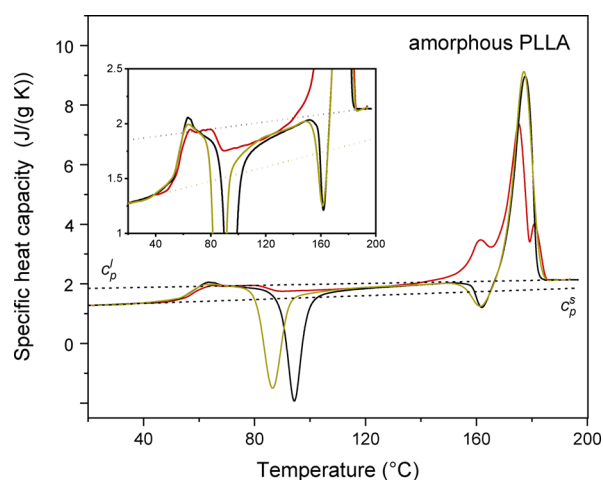


Figure 2. Apparent specific heat capacity ($c_{p,app}$) at the heating rate of 10 K/min (black line) and at the average heating rate of 2 K/min (yellow line), and reversing specific heat capacity ($c_{p,rev}$, red line) at the average heating rate of 2 K/min ($p = 120$ s) for amorphous PLLA. The inset is an enlargement of the $c_{p,app}$ and $c_{p,rev}$ curves. The black dotted lines are the thermodynamic solid and liquid specific heat capacities (c_p^s and c_p^l) of PLLA, adapted with permission from ref 44. Copyright (2005) American Chemical Society.

peak, the $c_{p,rev}$ curves display a sharp decrease due to the irreversible nature of the cold crystallization process and the increase in the crystalline fraction.⁴⁹ In the temperature range of the cold crystallization, mainly the α' -crystals grow,^{6–9} as also proven by the typical exothermic peak in the $c_{p,app}$ curves at about 160 °C, which is connected with the reorganization of the disordered α' -crystals into the more ordered α -form.^{10,11} At higher temperatures, the main melting observed in the $c_{p,app}$ curve is due to the fusion of the newly formed α -crystals. As the reversing heat capacity in the melting region originates from melting/crystallization processes that can be reversed by the temperature modulation, which generally do not involve the entire crystal fraction, the shape of the $c_{p,rev}$ peak is usually different from that of the $c_{p,app}$ curve.¹³

Figures 3 and 4 show the $c_{p,app}$ and $c_{p,rev}$ curves of the semicrystalline PLLA specimens after crystallization for different times at $T_{mold} = 95$ and 110 °C. Above the glass transition, in the range between 80 and 110 °C, a cold crystallization exotherm is observed in the $c_{p,app}$ curves after low molding times. The exotherm disappears for $t_{mold} \geq 30$ min at $T_{mold} = 95$ °C and $t_{mold} \geq 15$ min at $T_{mold} = 110$ °C,

which means that after these molding times, crystallization is almost complete or complete.

The comparison between the $c_{p,app}$ and $c_{p,rev}$ curves in the glass transition region shows that the T_g value from the $c_{p,rev}$ curves is higher than that from the $c_{p,app}$ curves after low molding times, i.e., in a condition of incomplete crystallization, according to the trend usually observed, as discussed above. The opposite behavior is observed after higher molding times when crystallization is almost complete or complete. (It is worth noting that similar $c_{p,app}$ curves are observed also at 2 K/min, as proven in Figures 3 and 4 for $T_{mold} = 95$ °C/ $t_{mold} = 40$ min and $T_{mold} = 110$ °C/ $t_{mold} = 20$ min.)

According to TMDSC fundamentals, $c_{p,rev}$ originates from the amplitude of the endothermic and exothermic events that follow the temperature modulation, occurring separately in the two semiperiods, whereas the latent heats released or absorbed sum algebraically in the apparent specific heat capacity.⁵⁰ If irreversible endothermic or exothermic events occurs simultaneously with the devitrification process, then the glass transition can be partially or completely masked in the $c_{p,app}$ curve and exhibit a shape completely different from the typical heat capacity step. On the other hand, the $c_{p,rev}$ curve is able to separate and resolve the glass transition, also in the presence of nonreversing events, because the glass transition is a reversing process that can follow the temperature modulation.⁴⁵ Thus, the $c_{p,rev}$ curve in the T_g region represents the baseline heat capacity,⁴⁵ which means that the difference between $c_{p,app}$ and $c_{p,rev}$ has to be associated to nonreversing processes that irreversibly absorb or release enthalpy.

The different shape of the $c_{p,app}$ and $c_{p,rev}$ curves in the T_g region, observed in Figures 3 and 4 after high molding times, can originate from the concomitant occurring of the glass transition and exothermic events, for example, a cold crystallization and/or an enthalpy release due to pressure and strain effects caused by the molding process.⁵¹ The presence of an exothermic event in the glass transition region has been reported for drawn PLLA with a draw ratio higher than 2 and explained as due to a strain-induced crystallization in the presence of oriented amorphous chains.^{52,53} Also in the PLLA specimens investigated in the present study, a certain unknown chain alignment can be produced during the processing by injection molding.^{54,55} However, the oriented amorphous chains are expected to relax, at least partially, at the quite high molding temperatures,⁵⁶ and certainly, the relaxation rate decreases as the crystallization proceeds due to constraints imposed by the newly formed crystals on the

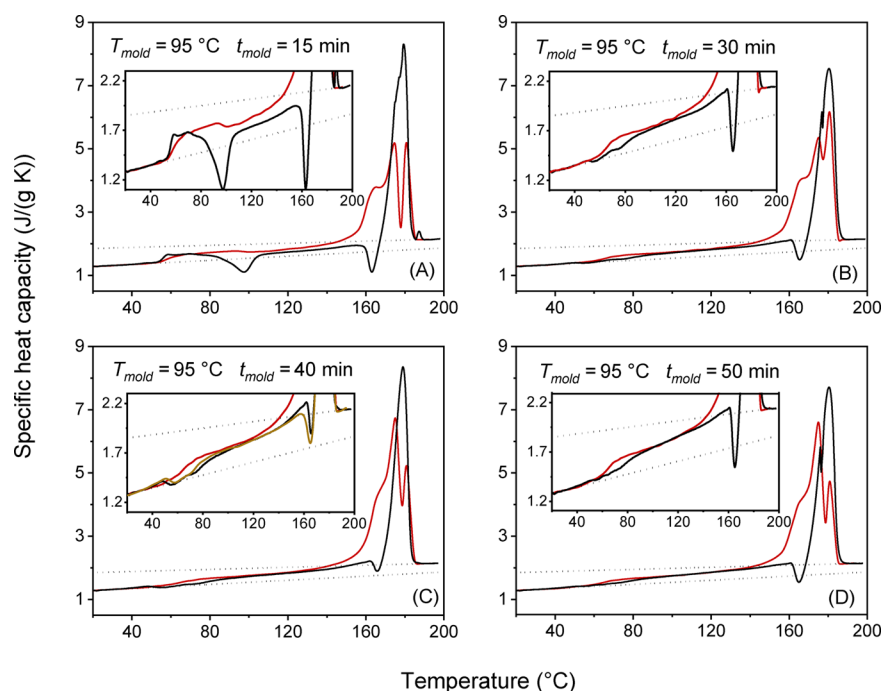


Figure 3. (A–D) Apparent specific heat capacity ($c_{p,app}$, black lines) at the heating rate of 10 K/min, and reversing specific heat capacity ($c_{p,rev}$, red lines) at the average heating rate of 2 K/min ($p = 120$ s) for PLLA after molding at $T_{mold} = 95$ °C for the indicated molding times (t_{mold}). The apparent specific heat capacity ($c_{p,app}$) at the average heating rate of 2 K/min (yellow line) is also shown for $t_{mold} = 40$ min. The insets are enlargements of the $c_{p,app}$ and $c_{p,rev}$ curves. The black dotted lines are the thermodynamic solid and liquid specific heat capacities (c_p^s and c_p^l) of PLLA, adapted with permission from ref 44. Copyright (2005) American Chemical Society.

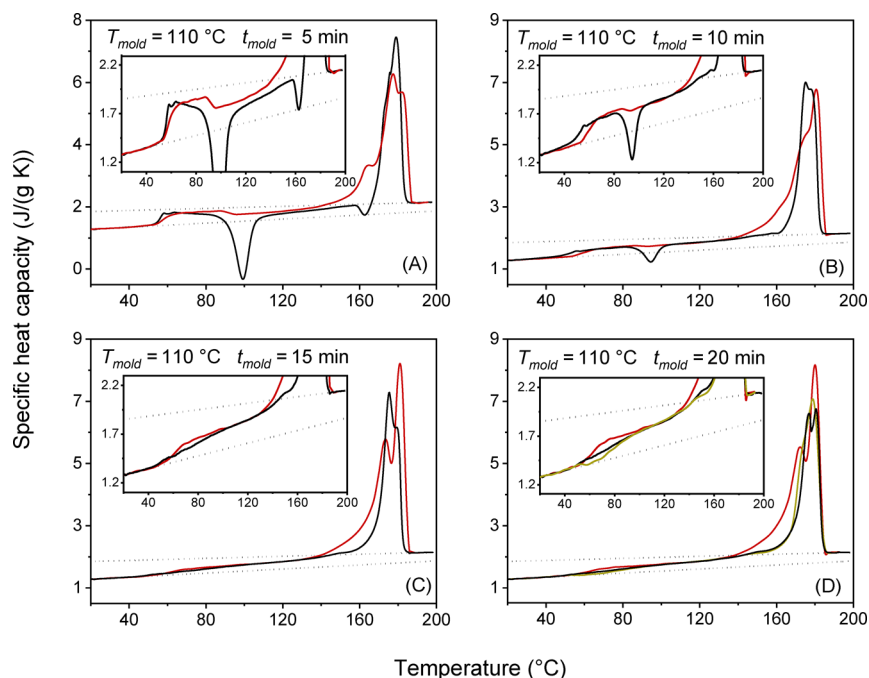


Figure 4. (A–D) Apparent specific heat capacity ($c_{p,app}$, black lines) at the heating rate of 10 K/min, and reversing specific heat capacity ($c_{p,rev}$, red lines) at the average heating rate of 2 K/min ($p = 120$ s) for PLLA after molding at $T_{mold} = 110$ °C for the indicated molding times (t_{mold}). The apparent specific heat capacity ($c_{p,app}$) at the average heating rate of 2 K/min (yellow line) is also shown for $t_{mold} = 20$ min. The insets are enlargements of the $c_{p,app}$ and $c_{p,rev}$ curves. The black dotted lines are the thermodynamic solid and liquid specific heat capacities (c_p^s and c_p^l) of PLLA, adapted with permission from ref 44. Copyright (2005) American Chemical Society.

close amorphous segments.⁵⁷ However, most likely, the exothermic event in proximity of the glass transition has to be ascribed to enthalpy relaxation because it is detected only after high molding times. It is known that exothermic peaks

can be caused by release of mechanically induced excess enthalpy.⁵¹ This event occurs when a pressure-densified glass relaxes to a less dense glass with lower enthalpy. The PLLA specimens molded for different times at $T_{mold} = 95$ and 110 °C,

after quick cooling to T_{room} , undergo volume and enthalpy adjustments as a consequence of both temperature and pressure decreases. These adaptations can be more favored at T_{room} in the unconstrained amorphous regions that characterize a semicrystalline material at the beginning of the crystallization process but can become hindered in an amorphous phase that experiences physical constraints imposed by the surrounding crystalline regions.^{14,57} This could explain why the enthalpy release is observed above T_{room} in the T_g region, only for the specimens almost completely or completely crystallized.

Figures 3 and 4 display that the melting behavior of PLLA is largely affected by the crystallization conditions. The exothermic peak at about 160 °C, connected with the reorganization of the disordered α' -crystals into the more stable α -form,^{10,11} is present in the $c_{p,\text{app}}$ curves of (i) PLLA crystallized at $T_{\text{mold}} = 95$ °C, because at this temperature, only α' -crystals grow, and (ii) PLLA crystallized at $T_{\text{mold}} = 110$ °C for $t_{\text{mold}} = 5$ min due to α' -crystals that develop during the cold crystallization process in the temperature range between 70 and 100 °C. It is worth noting that the melting peak is single if the crystallization process produces only original α' -crystals, which upon heating, transform into the more ordered α -phase so that the final melting peak is associated to the fusion of the newly crystallized α -crystals. Conversely, a double melting is observed in the presence of only α -crystals: the peak at lower temperatures is due to the fusion of original α -crystals, whereas the peak at higher temperature is due to the fusion of α -crystals recrystallized upon heating^{58,59} as, commonly, reorganization and recrystallization overlap the entire fusion process in semicrystalline polymers at a relatively low heating rate.⁶⁰

The T_g values for all the PLLA specimens, determined at half of the heat capacity increment of the $c_{p,\text{rev}}$ curves, are reported in Table 2. As expected, the T_g values of the semicrystalline PLLA appear higher than those of the amorphous PLLA, progressively increasing with t_{mold} . The slightly higher T_g values after crystallization at $T_{\text{mold}} = 95$ °C are in agreement with literature data¹⁴ and are ascribable to the devitrification of a mobile amorphous phase slightly more constrained with respect to the one that develops during crystallization at higher temperatures. This slightly constrained MAF has not to be confused with the rigid amorphous fraction, which mobilizes above the T_g region, being subjected to greater constraints.

The mobile amorphous weight fractions (X_{MAF}) were calculated at T_g as $X_{\text{MAF}} = \Delta c_p / \Delta c_p^a$, where Δc_p is the specific capacity increment from the $c_{p,\text{rev}}$ curves, and Δc_p^a is the specific heat capacity increment of the completely amorphous PLLA ($\Delta c_p^a = 0.52$ J/g K). Due to the presence of cold crystallization exotherms, with additional growth of both α' - and α -crystals with unknown percentages upon heating, a correct determination of the crystallinity degree is not attainable from all the $c_{p,\text{app}}$ curves, by taking into account the different enthalpy of melting values of 100% crystalline α' - and α -forms.⁶¹ Thus, the crystalline weight fractions were assumed equal to the crystal fractions obtained by XRD analysis, and the rigid amorphous weight fractions (X_{RAF}) were deduced by difference ($X_{\text{RAF}} = 1 - X_C - X_{\text{MAF}}$). All these data, listed in Table 2, show that for the two PLLA series crystallized at $T_{\text{mold}} = 95$ and 110 °C, the crystal fraction increases with the molding time, whereas in parallel, the mobile amorphous fraction decreases. The rigid amorphous fraction appears approximately independent of t_{mold} after crystallization at T_{mold}

= 95 °C, whereas it increases with X_C for $T_{\text{mold}} = 110$ °C. It has to be pointed out that the X_{RAF} values collected in Table 2 are calculated at T_g , and therefore, they include the rigid amorphous fraction that develops (i) during the crystallization at T_{mold} and (ii) during the successive cooling to T_{room} . For PLLA, it has been proven that the RAF amount that develops during isothermal crystallization decreases with increasing crystallization temperature;^{14,15} therefore, it can be supposed that after crystallization at $T_{\text{mold}} = 110$ °C, the rigid amorphous fraction mainly develops upon the successive cooling to T_{room} . A high rigid amorphous fraction approximately independent of the crystallization time and crystallinity degree has been reported in the literature after crystallization at low temperatures,^{62,63} in perfect agreement with the present trend for $T_{\text{mold}} = 95$ °C. Likely at low temperature, at the beginning of the crystallization process, the low mobility of the chains leads to the growth of very imperfect crystals, with a high RAF amount at the amorphous/crystal interfaces. As crystallization proceeds, the organization of the crystal phase slightly improves, which can lead to a decrease in the X_{RAF}/X_C ratio in bulk PLLA, as also reported for poly(3-hydroxybutyrate).⁶⁴ It is worth noting that a different X_{RAF}/X_C evolution has been observed for nanoconfined PLLA,⁶⁵ which proves that the crystal/amorphous coupling strongly depends on the geometrical dimensions of the sample under investigation. The present results demonstrate that formation of rigid amorphous fraction is favored at lower crystallization temperatures.

2.3. Tensile Characterization of Amorphous PLLA and after Different Crystallization Times at $T_{\text{mold}} = 95$ and 110 °C. The values of the experimental elastic modulus (E), tensile strength at break (TS), and elongation at break of PLLA, after crystallization at $T_{\text{mold}} = 95$ and 110 °C for different molding times, measured at T_{room} , are listed in Table 2. It can be noted that, with increasing molding time and, therefore, crystallinity, the elastic modulus slightly increases, whereas in parallel, the tensile strength and elongation at break decrease. For similar X_C values, the elastic modulus of the semicrystalline PLLA containing α' -crystals is lower than that of the samples containing α -crystals, whereas the tensile strength and elongation at break data are higher. The fracture behavior of all the PLLA semicrystalline specimens appears fragile, as typically reported for PLLA:^{1,66} the crystalline regions act as stress concentrators, which leads to premature failure of the materials. The value of the elastic modulus of PLLA in the glassy state at T_{room} is in perfect agreement with literature data.^{1,66}

To correlate the mechanical properties with the structure of semicrystalline PLLA, the crystalline, mobile amorphous, and rigid amorphous weight fractions listed in Table 2 were transformed into the corresponding volumetric fractions, V_C , V_{MAF} , and V_{RAF} , after determination of the respective density values.

The measurement of the density at $T_{\text{room}} = 21$ °C of (i) the amorphous PLLA ($\rho_{\text{MAF}} = 1.240 \pm 0.005$ g/cm³) and (ii) the semicrystalline PLLA crystallized at $T_{\text{mold}} = 95$ °C for $t_{\text{mold}} = 50$ min and at $T_{\text{mold}} = 110$ °C for $t_{\text{mold}} = 20$ min ($\rho = 1.225 \pm 0.005$ and 1.222 ± 0.005 g/cm³, respectively) allowed the determination of the density of the rigid amorphous fraction (ρ_{RAF}) according to the following relationship

$$\frac{1}{\rho} = \frac{X_C}{\rho_C} + \frac{X_{\text{MAF}}}{\rho_{\text{MAF}}} + \frac{X_{\text{RAF}}}{\rho_{\text{RAF}}} \quad (1)$$

Table 3. Crystalline (V_C) and Rigid Amorphous (V_{RAF}) Volume Fractions, Texture Parameters (λ and φ), Elastic Modulus of the Semicrystalline PLLA (E), and Elastic Modulus of the α' -Crystals (E_C) Predicted by eqs 2 and 3

t_{mold} at $T_{\text{mold}} = 95\text{ }^\circ\text{C}$ (min)	V_C	V_{RAF}	λ (eq 2)	λ (eq 3)	φ (eq 2)	φ (eq 3)	E (GPa) (eq 2)	E (GPa) (eq 3)	E_C (α') (GPa) (eq 2)	E_C (α') (GPa) (eq 3)
15	0.29	0.24	0.10	0.17	0.10	0.20	3.90	3.82		
30	0.37	0.24	0.10	0.18	0.10	0.21	3.90	3.84	3.9	13.1
40	0.38	0.24	0.10	0.18	0.10	0.21	3.90	3.84		
50	0.39	0.25	0.10	0.20	0.10	0.24	3.90	3.90		

Table 4. Crystalline (V_C) and Rigid Amorphous (V_{RAF}) Volume Fractions, Texture Parameters (λ and φ), Elastic Modulus of the Semicrystalline PLLA (E), and Elastic Modulus of the α -Crystals (E_C) Predicted by eqs 2 and 3

t_{mold} at $T_{\text{mold}} = 110\text{ }^\circ\text{C}$ (min)	V_C	V_{RAF}	λ (eq 2)	λ (eq 3)	φ (eq 2)	φ (eq 3)	E (GPa) (eq 2)	E (GPa) (eq 3)	E_C (α) (GPa) (eq 2)	E_C (α) (GPa) (eq 3)
5	0.18	0.08	0.20	0.21	0.20	0.22	4.18	4.00		
10	0.37	0.17	0.20	0.25	0.20	0.26	4.18	4.10	4.2	16.5
15	0.39	0.20	0.20	0.27	0.20	0.28	4.18	4.16		
20	0.41	0.22	0.20	0.34	0.20	0.28	4.18	4.34		

with the density of the crystalline α' - and α -phases (ρ_C) assumed equal to 1.245 and 1.265 g/cm³, respectively, as reported above. The density of the RAF connected with the α' -crystals turned out to be 1.17 g/cm³, approximately 3% lower than ρ_{MAF} , whereas the density of the RAF connected with the α -crystals came out to be 1.11 g/cm³, about 10% lower than ρ_{MAF} . To the best of our knowledge, this is the first determination of the RAF density for PLLA. The finding that ρ_{RAF} is lower than ρ_{MAF} is in perfect agreement with (i) theoretical expectations, because the higher vitrification temperature of the RAF induces a higher free volume in its glassy state with respect to the MAF,⁶⁷ and (ii) experimental evidence of de-densification occurring during crystallization.⁶⁸ Indeed, some studies have proven that in semicrystalline polymers, the rigid amorphous fraction has a significant and detrimental impact on the barrier properties because it counterbalances the positive influence of the crystalline regions.^{69,70} An important result of the present investigation is that the density of the RAF linked to the more ordered α -crystals is lower with respect to that of the RAF connected to the conformationally disordered α' -modification. It is likely that the tight chain arrangement of the α -form produces a higher stress and stronger coupling at the amorphous/crystal interface, which hinders significantly the relaxation of the amorphous segments, so that a higher free volume remains trapped in proximity of the crystals.

By assuming the density data above reported, the calculated V_C , V_{MAF} , and V_{RAF} values turned out to be substantially equal to the X_C , X_{MAF} , and X_{RAF} data listed in Table 2 (see Tables 3–6).

2.4. Modeling of the Elastic Modulus of the Rigid Amorphous Fraction and α' - and α -Phases of PLLA. A simple schematization of the original two-phase Takayanagi model is reported in Figure 5. Different arrangements can be assumed. In the series–parallel models (Figure 5a,c), which represent a situation of good stress transfer normal to the applied tensile stress, the strain of phase 2 is equal to that of the element close to it, whereas in the parallel–series models (Figure 5b,d), the strain of phase 2 is different from that of the other elements due to poor stress transfer. The combinations shown in Figure 5c,d represent situations with the crystalline domains dispersed in the continuous amorphous phase, which holds especially for semicrystalline polymers with a low or intermediate crystallinity degree, whereas the models depicted

Table 5. Crystalline (V_C) and Rigid Amorphous (V_{RAF}) Volume Fractions, Texture Parameters (β and γ), Elastic Modulus of the Semicrystalline PLLA (E), Elastic Modulus of the α' -Crystals (E_C), and Elastic Modulus of the RAF (E_{RAF}) Connected to α' -Crystals Predicted by eq 4

t_{mold} at $T_{\text{mold}} = 95\text{ }^\circ\text{C}$ (min)	V_C	V_{RAF}	γ (eq 4)	β (eq 4)	E (GPa) (eq 4)	E_C (α') (GPa) (eq 4)	E_{RAF} (GPa) (eq 4)
15	0.29	0.24	0.21	0.11	3.82		
30	0.37	0.24	0.22	0.13	3.84	11.2	5.4
40	0.38	0.24	0.22	0.16	3.84		
50	0.39	0.25	0.27	0.18	3.91		

Table 6. Crystalline (V_C) and Rigid Amorphous (V_{RAF}) Volume Fractions, Texture Parameters (β and γ), Elastic Modulus of the Semicrystalline PLLA (E), Elastic Modulus of the α -Crystals (E_C), and Elastic Modulus of the RAF (E_{RAF}) Connected to α -Crystals Predicted by eq 4

t_{mold} at $T_{\text{mold}} = 110\text{ }^\circ\text{C}$ (min)	V_C	V_{RAF}	γ (eq 4)	β (eq 4)	E (GPa) (eq 4)	E_C (α) (GPa) (eq 4)	E_{RAF} (GPa) (eq 4)
5	0.18	0.08	0.20	0.11	3.94		
10	0.37	0.17	0.25	0.16	4.08	14.8	6.1
15	0.39	0.20	0.28	0.23	4.17		
20	0.41	0.22	0.29	0.26	4.37		

in Figure 5a,b describe the opposite condition with high crystal content. It was proven that the models shown in Figure 5a,c are more suitable for the calculation of the equivalent elastic modulus of semicrystalline polymers because they better interpret the strain distribution under stress in these materials.^{30–35} Thus, only these latter arrangements are considered here.

The equations that allow the calculation of the elastic modulus, according to the model described in Figure 5a,c are respectively

$$\frac{1}{E} = \frac{1 - \lambda}{E_C} + \frac{\lambda}{\varphi E_A + (1 - \varphi) E_C} \quad (2)$$

$$\frac{1}{E} = \frac{1 - \lambda}{E_A} + \frac{\lambda}{\varphi E_C + (1 - \varphi) E_A} \quad (3)$$

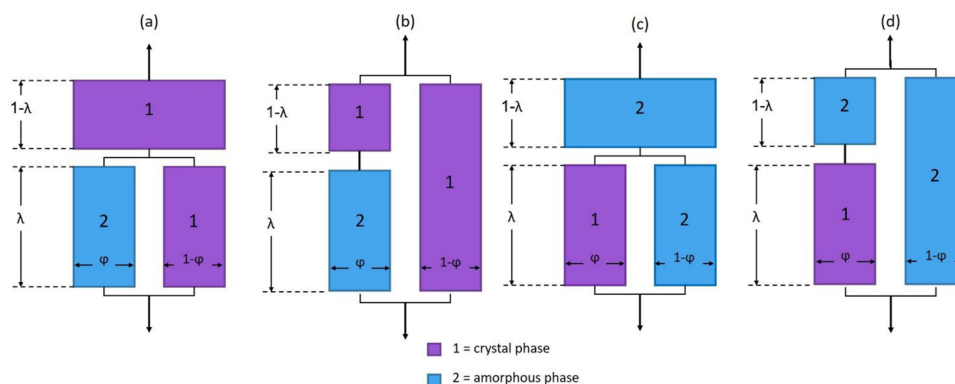


Figure 5. (a–d) Schematic representation of the two-phase Takayanagi mechanical models of semicrystalline polymers.

where E , E_C , and E_A are the elastic moduli of the semicrystalline polymer, crystal phase, and amorphous phase, respectively, whereas λ and φ , which range between 0 and 1, are texture parameters connected with the phase composition and related to the degree of parallel and series coupling of the two phases, respectively. In the original Takayanagi treatment, a spherical shape was assumed for the dispersed phase. According to this supposition, the product $\varphi \cdot \lambda$ equals the volume fraction of the dispersed phase, i.e., the amorphous phase or crystal phase according to the models depicted in Figure 5a,c, respectively. To avoid the recourse to this approximation, a preliminary estimation of the texture parameters for the two-phase models shown in Figure 5a,c was performed by means of an iterative numerical method (using Excel Data Solver Function). Experimental evidence reported in the literature has suggested that the elastic modulus of the RAF is higher than that of the MAF and probably closer to that of the crystal phase;^{19–27} thus, as a first approximation, a single block containing these two fractions was assumed due to the tight connection between the crystal phase and RAF. Consequently, the φ texture parameter becomes connected to the mechanical response of the amorphous fraction or the coupled crystalline and rigid amorphous fractions. A minimization of the mean square error between the experimental and theoretical elastic moduli predicted by eqs 2 and 3 was carried out for the semicrystalline PLLA containing α' - and α -crystals to calculate the parameters λ , φ , and E_C by keeping the experimental elastic modulus of the amorphous phase fixed ($E_A = 3.6$ GPa). The final results of the mathematical iterations for the two semicrystalline PLLA series are reported in Tables 3 and 4, respectively.

Tables 3 and 4 show that the λ , φ , and E_C values obtained by applying eq 2, which is related to the mechanical configuration of Figure 5a, are not realistic because the calculated E_C data are close to E_A and much lower than the experimental and theoretical E_C values reported in the literature,¹⁸ although a combined lower contribution of the RAF is expected. Furthermore, the values of the texture parameters (λ and φ), as well as the predicted E values, are not coherent as they do not vary with t_{mold} and, consequently, with the phase composition. Actually, λ and φ must necessarily vary with the phase composition due to change in the crystalline and amorphous phase block extension. These results demonstrate that the model depicted in Figure 5a, theorized for polymers having a dominant crystalline phase, is not suitable to describe the present PLLA semicrystalline systems. Conversely, the model shown in Figure 5c provides more coherent data not

only of the crystalline elastic moduli, which are very close to experimental and theoretical data found in the literature, but also of the texture parameters and the predicted E values, which increase with the crystal content.

This two-phase representation is however still imprecise because the separate and different contribution of the RAF is not taken into consideration. Thus, the Takayanagi model was modified by inserting the RAF block between the MAF and the crystal blocks. The configuration adopted for the three-phase model, already applied successfully to poly(3-hydroxybutyrate-co-3-hydroxyvalerate) copolymers, is shown in Figure 6. Two

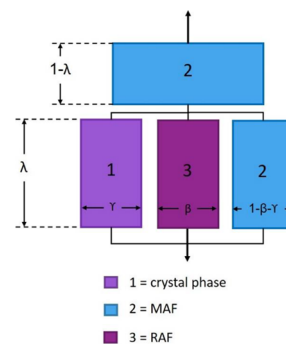


Figure 6. Schematic representation of the three-phase Takayanagi mechanical models of semicrystalline polymers.

texture parameters, β and γ , correlated to the RAF and crystal phase, respectively, were introduced. The equation that describes the equivalent elastic modulus of the semicrystalline polymer according to the configuration of Figure 6 is

$$\frac{1}{E} = \frac{1-\lambda}{E_{\text{MAF}}} + \frac{\lambda}{\gamma E_C + \beta E_{\text{RAF}} + (1-\gamma-\beta)E_{\text{MAF}}} \quad (4)$$

An iterative process was again carried out by minimizing the mean square error between the experimental and theoretical elastic moduli predicted by eq 4, with the aim of calculating the parameters β , γ , E_C , and E_{RAF} , having the experimental elastic modulus of the amorphous phase ($E_{\text{MAF}} = 3.6$ GPa) fixed, as well as the parameter λ , calculated via eq 3 and listed in Tables 3 and 4. The results of the minimization procedure are reported in Tables 5 and 6 for the α' - and α -phases, respectively.

The results obtained are in excellent agreement with intuitive expectation because the modulus of rigid amorphous fraction is found to be lower than that of the crystal phase for both the α' - and α -crystals. This trend can be rationalized by

considering that, with respect to the crystal phase, higher free volume and weaker intermolecular bonding can favor chain rearrangement under stress in the RAF regions. It is worth noting that at T_{room} at which the experimental elastic moduli were measured, all the three fractions of PLLA (crystalline, mobile amorphous, and rigid amorphous) are solid. With respect to the RAF, the mobile amorphous fraction in the glassy state is characterized by a lower free volume but also by fewer physical constraints. This latter property can explain the slightly higher E_{RAF} value with respect to the experimental elastic modulus of the MAF.

Very impressive are the values of the elastic moduli of the two crystalline forms of PLLA. The calculated E_C data are in perfect agreement with the experimental and theoretical evaluation of the ultimate elastic modulus of the α' - and α -forms of PLLA (12.6 and 12.9 GPa for the α' -form and 13.8 and 14.7 GPa for the α -form).¹⁸ Polymer crystals generally exhibit mechanical anisotropy, with the highest modulus in the chain axis direction and lower moduli in the other directions.⁷¹ For PLLA, the elastic modulus of the α -phase was found approximately constant in all the directions, whereas a stronger anisotropy was detected for the α' -modification.¹⁸ This can explain the slightly lower E_C value here derived for the α' -phase with respect to the theoretical and experimental data by taking into account the different orientations of the real crystals with respect to the load direction.

The very good correspondence between the E_C values determined from the three-phase Takayanagi mechanical model and the experimental and theoretical values reported in the literature for the α' - or α -crystals constitutes a proof of the validity and reliability of the derived E_{RAF} data. Interestingly, the values of the elastic modulus of the RAF linked to the α -form turned out to be slightly higher with respect to RAF connected to the disorder α' -phase, likely due to the stronger constraints imposed by the more ordered crystalline form.

Finally, Tables 5 and 6 show also that the texture parameters β and γ , determined with no empirical assumptions, increase with the crystalline and RAF amounts, confirming that these parameters are correctly connected with the extensions of the different blocks, i.e., with the composition of the semicrystalline polymer and the fractions of the different phases.

The comparison between the experimental moduli of the semicrystalline PLLA specimens containing α' - and α -crystals and the values predicted by the three-phase Takayanagi model (eq 4) is shown in Figure 7. As all the fractions (crystalline, mobile amorphous, and rigid amorphous) together influence the elastic modulus and the relationship between E and E_C and E_{RAF} is complex, the calculated E values are reported separately as functions of the crystalline and rigid amorphous volume fractions. The graphical comparison proves that the three-phase Takayanagi model describes satisfactorily the experimental E data of semicrystalline PLLA samples.

3. CONCLUSIONS

In the present study, the evolution of the mechanical properties of semicrystalline PLLA after different crystallization times at $T_{\text{mold}} = 95$ and 110 °C has been investigated. The two different crystallization temperatures allowed us to obtain samples containing exclusively α' - and α -crystals, as proven by XRD analysis.

In particular, the connection between the measured elastic modulus and phase composition of the semicrystalline samples

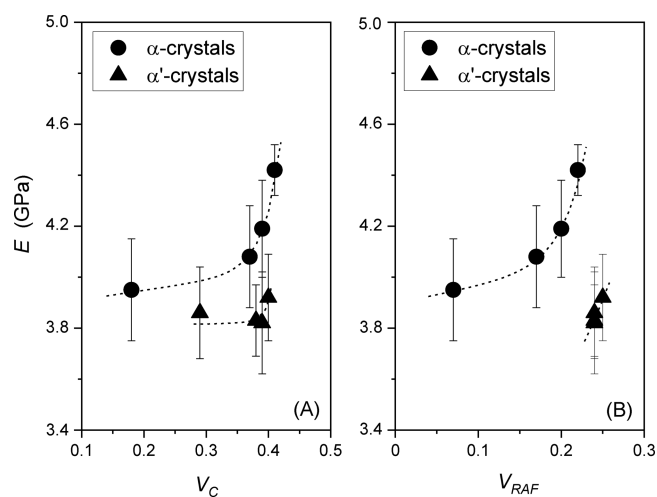


Figure 7. Comparison between the experimental elastic moduli of semicrystalline PLLA containing α' - and α -crystals and the values predicted by the three-phase modified Takayanagi model (dotted lines) as a function of (A) the crystalline volume fraction (V_C) and (B) the rigid amorphous volume fraction (V_{RAF}). The bars are the experimental errors.

has been analyzed in detail. The crystalline, mobile amorphous, and rigid amorphous fractions for all the samples have been quantified by combined XRD, DSC, and TMDSC measurements. With increasing molding time and, therefore, the crystallinity, the elastic modulus was found to slightly increase, whereas in parallel, the tensile strength and elongation at break decreased. For a similar crystallinity degree, the elastic modulus of the semicrystalline PLLA containing α' -crystals turned out to be lower than that of the samples containing α -crystals, in agreement with experimental and theoretical evaluation of the ultimate elastic modulus of the α - and α' -forms of PLLA.¹⁸ It is known that the possible presence of polymorphism can influence the physical and mechanical properties of semicrystalline polymers because different polymorphic forms of the same polymer may show completely different physical and mechanical properties.^{16,17} This means that the crystallization conditions can markedly control and tailor the final performance of these materials. Actually, a complete interpretation of the physical properties of semicrystalline polymers must take into account not only the crystal phase and mobile amorphous fraction but also the constrained amorphous interphase or rigid amorphous fraction contribution.

The novelty proposed by the present study is the estimation of the elastic modulus at T_{room} of the rigid amorphous fraction connected to PLLA α' - and α -crystals, respectively. The calculations have been performed on the basis of a mechanical model widely applied to semicrystalline polymers, which has been here transformed into a three-phase approach. The procedure, which allows the simultaneous quantification of the elastic moduli of the RAF and the crystalline fraction, led to E_C values for the α' - and α -phases (11.2 and 14.8 GPa, respectively), in excellent agreement with the corresponding experimental and theoretical values reported in the literature, with the difference between the two forms interpreted as due to dissimilar chain conformation regularity and lattice dimensions. Also, the elastic moduli of the RAF linked to the disordered α' -form were found to be slightly lower with respect to RAF connected to the α -phase (5.4 and 6.1 GPa,

respectively), likely due to the stronger constraints imposed by the more ordered α -crystalline form. Thus, the elastic moduli at T_{room} of the crystalline, mobile amorphous, and rigid amorphous fractions of PLLA turned out to be quantitatively in the order of $E_{\text{MAF}} < E_{\text{RAF}} < E_{\text{C}}$, with the experimental E_{MAF} value equal to 3.6 GPa. The trend appears to be totally in agreement with experimental results and theoretical expectations: the fewer physical constraints that characterize the mobile amorphous fraction, which is in the glassy state at T_{room} , with respect to the rigid amorphous fraction can explain the lower E_{MAF} value with respect to the derived elastic modulus of the RAF. On the other hand, the much weaker intermolecular bonding and higher free volume of the constrained RAF regions with respect to the crystal phase can better favor chain rearrangement under stress and leads to E_{RAF} values considerably lower than the E_{C} data.

4. MATERIALS AND METHODS

4.1. Materials. Commercial PLA granules derived from natural resources, purchased from NatureWorks LLC, were used. PLA Ingeo 3100HP, containing 0.3% of D-lactic acid units [melt flow index (MFR): 24 g/10 min (210 °C, 2.16 kg); nominal average molar mass: 120,000 g/mol; density: 1.24 g/cm³] is a PLA grade designed to crystallize during processing in most conventional injection molding equipment. As the commercial PLA used in the present study is a L-isomer-rich copolymer, the abbreviation PLLA is used.

The granules were dried in a Piovan DP 604-615 dryer at 60 °C before the injection molding, which was carried out using a Megatech H10/18 injection molding machine, to obtain Haake Type 3 dog-bone specimens (width: 5 mm; length: 25 mm; thickness: 1.5 mm). Amorphous and semicrystalline PLLA specimens were prepared by varying the molding temperature (T_{mold}) and molding time (t_{mold}). The molding temperatures were chosen to prepare specimens containing exclusively either α' - or α -crystals with t_{mold} values as small as possible. The operative parameters of the injection molding process are reported in Table 7. After processing, the PLLA specimens were quickly cooled to T_{room} in less than 1 min by means of cold air.

Table 7. Operating Conditions Used for the Injection Molding Process of the PLLA Specimens

condition	amorphous PLLA	semicrystalline PLLA α' -crystals	semicrystalline PLLA α -crystals
temperature of the feeder/injection zone (°C)	190/195	190/195	190/195
injection holding time (s)	15	15	15
injection pressure (bar)	80	80	80
molding temperature (T_{mold}) (°C)	50	95	110
molding time (t_{mold}) (min)	<1	15–30–40–50	5–10–15–20

After preparation, all the Haake Type 3 dog-bone specimens were stored in a climatic chamber at room temperature, in conditions of relative humidity of 50%, and analyzed after 3 days by differential scanning calorimetry (DSC), temperature-modulated differential scanning calorimetry (TMDSC), X-ray diffraction analysis (XRD), and mechanical testing.

4.2. X-ray Diffraction (XRD) Analysis. XRD patterns were collected at T_{room} using a PANalytical X'PertPro diffractometer in reflection mode, equipped with copper radiation ($\lambda = 0.15418$ nm) and a fast solid-state X'Celerator detector. The X-ray crystal fraction (X_{C}) was calculated as the ratio of the areas of the crystalline peaks and the total area of the background-corrected diffraction profile. To take into account the air and incoherent scattering, a scan without a sample was performed and properly scaled for each scan. The lattice constants were calculated from the positions of the most intense reflections by least-squares refinements.

4.3. Thermal Characterization by Differential Scanning Calorimetry (DSC) and Temperature-Modulated Differential Scanning Calorimetry (TMDSC). DSC and TMDSC measurements were performed with a PerkinElmer Calorimeter DSC 8500 equipped with an IntraCooler III as refrigerating system. The instrument was calibrated in temperature with high-purity standard materials (indium, naphthalene, and cyclohexane) at zero heating rate according to the procedure for conventional DSC.⁷² Enthalpy calibration was performed with indium. To gain precise apparent specific heat capacity data ($c_{\text{p,app}}$) from the heat flow rate signal, each scan was accompanied by an empty pan run (blank run). The mass of the blank and sample aluminum pans matched within 0.02 mg. To minimize the instrumental thermal lag, the sample mass was lower than 10 mg. Dry nitrogen was used as purge gas at a rate of 30 mL/min. The temperature of the samples during heating was corrected for the thermal lag, determined as the average by using different standard materials. This lag was 0.05 min, which for the heating rates of 2 and 10 K/min, corresponds to a temperature correction of -0.1 , and -0.5 K, respectively.

The PLLA specimens prepared by injection molding were analyzed (i) by conventional DSC from 20 to 200 °C at the heating rate of 10 K/min to obtain apparent specific heat capacity ($c_{\text{p,app}}$) curves and (ii) by TMDSC, with a saw-tooth modulation temperature program, at the average heating rate of 2 K/min, with a temperature amplitude (A_{T}) of 0.5 K and a modulation period (p) of 120 s, to obtain apparent specific heat capacity ($c_{\text{p,app}}$) curves and reversing specific heat capacity ($c_{\text{p,rev}}$) curves. According to the mathematical treatment of TMDSC data, the modulated temperature and heat flow rate curves can be approximated to discrete Fourier series and separated into underlying and periodic components.^{73,74} The underlying components are equivalent to the conventional linear program of the temperature and corresponding conventional heat flow rate signal, from which the $c_{\text{p,app}}$ curve can be derived. Conversely, from the periodic component, the $c_{\text{p,rev}}$ curve is calculated according to the following equation

$$c_{\text{p,rev}}(\omega, T) = \frac{A_{\text{HF}}(T) K(\omega)}{A_{\text{T}}(T) m\omega} \quad (5)$$

where A_{HF} and A_{T} are the amplitudes of the first harmonic of the modulated heat flow and temperature, respectively, ω is the fundamental frequency of temperature modulation ($\omega = 2\pi/p$), m is the mass of the sample, and $K(\omega)$ is the frequency-dependent calibration factor. The average $K(\omega)$ values, determined by calibration with sapphire, was 1.00 ± 0.02 for $p = 120$ s.

4.4. Tensile Characterization. Tensile tests on the PLLA specimens were carried out at T_{room} with a crosshead speed of 10 mm/min, by means of an Instron universal testing machine

5500R equipped with a 10 kN load cell and interfaced with a computer running MERLIN software (INSTRON version 4.42 S/N-014733H). At least 10 specimens were tested for each sampling and the average values were reported.

4.5. Density Measurements. Density measurements were performed by means of an analytic balance Sartorius RC 210 D (0.01 mg resolution), equipped with the density determination kit YDK 01-0D, in accordance with ASTM D792 (Standard Test Methods for Density and Specific Gravity of Plastics by Displacement). The density values, determined at $T_{\text{room}} = 21$ °C, were obtained as the average of at least 20 measurements.

AUTHOR INFORMATION

Corresponding Authors

Andrea Lazzeri – Department of Civil and Industrial Engineering, University of Pisa, Pisa 56122, Italy; CNR-IPCF, National Research Council–Institute for Chemical and Physical Processes, Pisa 56124, Italy; orcid.org/0000-0002-9463-1502; Email: andrea.lazzeri@unipi.it

Maria Cristina Righetti – CNR-IPCF, National Research Council–Institute for Chemical and Physical Processes, Pisa 56124, Italy; orcid.org/0000-0002-0484-7482; Email: cristina.righetti@pi.ipcf.cnr.it

Authors

Laura Aliotta – Department of Civil and Industrial Engineering, University of Pisa, Pisa 56122, Italy; orcid.org/0000-0003-1876-5995

Massimo Gazzano – CNR-ISOF, National Research Council–Institute of Organic Synthesis and Photoreactivity, Bologna 40129, Italy; orcid.org/0000-0003-1352-9547

Complete contact information is available at:

<https://pubs.acs.org/10.1021/acsoomega.0c02330>

Author Contributions

The manuscript was written through contributions of all authors. All authors have given approval to the final version of the manuscript.

Notes

The authors declare no competing financial interest.

REFERENCES

- (1) Anderson, K. S.; Schreck, K. M.; Hillmyer, M. A. Toughening Poly(lactide). *Polym. Rev.* **2008**, *48*, 85–108.
- (2) Saeidloua, S.; Huneaulta, M. A.; Li, H.; Park, C. B. Poly(lactic acid) Crystallization. *Progr. Polym. Sci.* **2012**, *37*, 1657–1677.
- (3) Urayama, H.; Kanamori, T.; Kimura, Y. Microstructure and Thermomechanical Properties of Glassy Poly(lactides) with Different Optical Purity of the Lactate Units. *Macromol. Mater. Eng.* **2001**, *286*, 705–713.
- (4) Pan, P.; Inoue, Y. Polymorphism and Isomorphism in Biodegradable Polyesters. *Progr. Polym. Sci.* **2009**, *34*, 605–640.
- (5) Wasanaku, K.; Tashiro, K. Crystal Structure and Disorder in Poly(l-lactic acid) δ form (α' form) and the Phase Transition Mechanism to the Ordered α form. *Polymer* **2011**, *52*, 6097–6109.
- (6) Kawai, T.; Rahman, N.; Matsuba, G.; Nishida, K.; Kanaya, T.; Nakano, M.; Okamoto, H.; Kawada, J.; Usuki, A.; Honma, N.; Nakajima, K.; Matsuda, M. Crystallization and Melting Behavior of Poly(l-lactic acid). *Macromolecules* **2007**, *40*, 9463–9469.
- (7) Pan, P.; Zhu, B.; Kai, W.; Dong, T.; Inoue, Y. Polymorphic Transition in Disordered poly(l-lactide) Crystals Induced by Annealing at Elevated Temperatures. *Macromolecules* **2008**, *41*, 4296–4304.
- (8) Pan, P.; Zhu, B.; Kai, W.; Dong, T.; Inoue, Y. Effect of Crystallization Temperature on Crystal Modifications and Crystal-

lization Kinetics of Poly(l-lactide). *J. Appl. Polym. Sci.* **2008**, *107*, 54–62.

(9) Zhang, J.; Tashiro, K.; Tsuji, H.; Domb, A. J. Disorder-to-Order Phase Transition and Multiple Melting Behavior of Poly(l-lactide) Investigated by Simultaneous Measurements of WAXS and DSC. *Macromolecules* **2008**, *41*, 1352–1357.

(10) Androsch, R.; Schick, C.; Di Lorenzo, M. L. Melting of Conformationally Disordered Crystals α' -phase of poly(l-lactic acid). *Macromol. Chem. Phys.* **2014**, *215*, 1134–1139.

(11) Hu, J.; Wang, J.; Bhoje Gowd, E.; Yuan, Y.; Zhang, T.; Duan, Y.; Hu, W.; Zhang, J. Small- and Wide-Angle X-ray Scattering Study on α' -to- α Transition of Poly(l-lactide acid) Crystals. *Polymer* **2019**, *167*, 122–129.

(12) Righetti, M. C. Amorphous Fractions of Poly(lactic acid). *Adv. Polym. Sci.* **2018**, *279*, 195–234.

(13) Wunderlich, B. Reversible Crystallization and the Rigid Amorphous Phase in Semicrystalline Macromolecules. *Progr. Polym. Sci.* **2003**, *28*, 383–450.

(14) Righetti, M. C.; Prevosto, D.; Tombari, E. Time and Temperature Evolution of the Rigid Amorphous Fraction and Differently Constrained Amorphous Fractions in PLLA. *Macromol. Chem. Phys.* **2016**, *217*, 2013–2026.

(15) Righetti, M. C.; Tombari, E. Crystalline, Mobile Amorphous and Rigid Amorphous Fractions in Poly(l-lactic acid) by TMDSC. *Thermochim. Acta* **2011**, *522*, 118–127.

(16) Tashiro, K. Molecular Theory of Mechanical Properties of Crystalline Polymers. *Progr. Polym. Sci.* **1993**, *18*, 377–435.

(17) De Rosa, C.; Scoti, M.; Di Girolamo, R.; Ruiz de Ballesteros, O.; Auriemma, F.; Malafronte, A. Polymorphism in Polymers: A Tool to Tailor Material's Properties. *Polym. Cryst.* **2020**, *3*, No. e10101.

(18) Wasanasuk, K.; Tashiro, K. Theoretical and Experimental Evaluation of Crystallite Moduli of Various Crystalline Forms of Poly(l-lactic acid). *Macromolecules* **2012**, *45*, 7019–7026.

(19) Rastogi, R.; Vellinga, W. P.; Rastogi, S.; Schick, C.; Meijer, H. E. H. The Three-Phase Structure and Mechanical Properties of Poly(ethylene terephthalate). *J. Polym. Sci., Part B: Polym. Phys.* **2004**, *42*, 2092–2106.

(20) Di Lorenzo, M. L.; Righetti, M. C. The Three-Phase Structure of Isotactic Poly(1-butene). *Polymer* **2008**, *49*, 1323–1331.

(21) Kolesov, I.; Androsch, R. The Rigid Amorphous Fraction of Cold-Crystallized Polyamide 6. *Polymer* **2012**, *53*, 4770–4777.

(22) Martin, S.; Exposito, M. T.; Vega, J. F.; Martinez-Salazar, J. Microstructure and Properties of Branched Polyethylene: Application of a Three-Phase Structural Model. *J. Appl. Polym. Sci.* **2013**, *128*, 1871–1878.

(23) Nguyen, T. L.; Bédoui, F.; Mazeran, P.-E.; Guigon, M. Mechanical Investigation of Confined Amorphous Phase in Semicrystalline Polymers: Case of PET and PLA. *Polym. Eng. Sci.* **2015**, *55*, 397–405.

(24) in 't Veld, P. J.; Hütter, M.; Rutledge, G. C. Temperature-Dependent Thermal and Elastic Properties of the Interlamellar Phase of Semicrystalline Polyethylene by Molecular Simulation. *Macromolecules* **2006**, *39*, 439–447.

(25) Sedighiamiri, A.; Van Erp, T. B.; Peters, G. W. M.; Govaert, L. E.; Van Dommelen, J. A. W. Micromechanical Modeling of the Elastic Properties of Semicrystalline Polymers: A Three-Phase Approach. *J. Polym. Sci., Part B: Polym. Phys.* **2010**, *48*, 2173–2184.

(26) Ghazavizadeh, A.; Rutledge, G. C.; Atai, A. A.; Ahzi, S.; Rémond, Y.; Soltani, N. Micromechanical Characterization of the Interphase Layer in Semi-crystalline Polyethylene. *J. Polym. Sci. Polym. Phys.* **2013**, *51*, 1228–1243.

(27) Gueguen, O.; Ahzi, S.; Makradi, A.; Belouettar, S. A New Three-Phase Model to Estimate the Effective Elastic Properties of Semi-Crystalline Polymers: Application to PET. *Mech. Mater.* **2010**, *42*, 1–10.

(28) Ahmed, S.; Jones, F. R. A Review of Particulate Reinforcement Theories for Polymer Composites. *J. Mater. Sci.* **1990**, *25*, 4933–4942.

- (29) Halpin, J. C.; Kardos, J. L. Moduli of Crystalline Polymers Employing Composite Theory. *J. Appl. Phys.* **1972**, *43*, 2235–2241.
- (30) Takayanagi, M.; Uemura, S.; Minami, S. Application of Equivalent Model Method to Dynamic Rheo-Optical Properties of Crystalline Polymer. *J. Polym. Sci., Part C: Polym. Symp.* **1964**, *5*, 113–122.
- (31) Takayanagi, M.; Imada, K.; Kajiyama, T. Mechanical Properties and Fine Structure of Drawn Polymers. *J. Polym. Sci., Part C: Polym. Symp.* **1966**, *15*, 263–281.
- (32) Bouquerel, F.; Bourgin, P.; Perez, J. Viscoelastic Behavior of Thin Bioriented Poly(ethylene terephthalate) Films Under Low and Medium Stresses. *Polymer* **1992**, *33*, 516–525.
- (33) de Oca, H. M.; Ward, I. M. Structure and Mechanical Properties of PGA Crystals and Fibres. *Polymer* **2006**, *47*, 7070–7077.
- (34) Lai, C.; Ayer, R.; Hiltner, A.; Baer, E. Effect of Confinement on the Relaxation of Poly(ethylene oxide). *Polymer* **2010**, *51*, 1820–1829.
- (35) Aliotta, L.; Cinelli, P.; Coltelli, M. B.; Righetti, M. C.; Gazzano, M.; Lazzeri, A. Effect of Nucleating Agents on Crystallinity and Properties of Poly(lactic acid) (PLA). *Eur. Polym. J.* **2017**, *93*, 822–832.
- (36) Woo, E. M.; Su, C. C.; Kuo, J.-F.; Seferis, J. C. Model with Experimental Evidences for the Morphology of Binary Blends of a Thermosetting Polycyanate with Thermoplastics. *Macromolecules* **1994**, *27*, 5291–5296.
- (37) Parulekar, Y.; Mohanty, A. K. Biodegradable Toughened Polymers from Renewable Resources: Blends of Polyhydroxybutyrate with Epoxidized Natural Rubber and Maleated Polybutadiene. *Green Chem.* **2006**, *8*, 206–213.
- (38) Stanford, J. L.; Young, R. J.; Day, R. J. Formation and Properties of Urethane Diacetylene Segmented Block Copolymers. *Polymer* **1991**, *32*, 1713–1725.
- (39) Hearle, J. W. S.; Prakash, R.; Wilding, M. A. Prediction of Mechanical Properties of Nylon and Polyester Fibers as Composites. *Polymer* **1987**, *28*, 441–448.
- (40) Lia, F.; Gao, Y.; Jiang, W. Design of High Impact Thermal Plastic Polymer Composites with Balanced Toughness and Rigidity: Toughening with One Phase Modifier. *Polymer* **2019**, *170*, 101–106.
- (41) Loos, M. R.; Manas-Zloczower, I. Reinforcement Efficiency of Carbon Nanotubes – Myth and Reality. *Macromol. Theory Simul.* **2012**, *21*, 130–137.
- (42) Zare, Y.; Rhee, K. Y. Accounting the Reinforcing Efficiency and Percolating Role of Interphase Regions in Tensile Modulus of Polymer/CNT Nanocomposites. *Eur. Polym. J.* **2017**, *87*, 389–397.
- (43) Righetti, M. C.; Aliotta, L.; Mallegni, N.; Gazzano, M.; Passaglia, E.; Cinelli, P.; Lazzeri, A. Constrained Amorphous Interphase and Mechanical Properties of Poly(3-Hydroxybutyrate-co-3-Hydroxyvalerate). *Front. Chem.* **2019**, *7*, 790.
- (44) Pyda, M.; Wunderlich, B. Reversing and Non-Reversing Heat Capacity of Poly(lactic acid) in the Glass Transition Region by TMDSC. *Macromolecules* **2005**, *38*, 10472–10479.
- (45) Schick, C. Temperature Modulated Differential Scanning Calorimetry (TMDSC)—Basics and applications to polymers. In *Handbook of Thermal Analysis and Calorimetry*; Cheng, S. Z. D., Ed.; Elsevier Science B.V.: Amsterdam, The Netherlands, 2002; Volume 3, p 713.
- (46) Lacey, A. A.; Price, D. M.; Reading, M. Theory and Practice of Modulated Temperature Differential Scanning Calorimetry. In *Modulated Temperature Differential Scanning Calorimetry*; Reading, M. D. J., Hourston, D. J., Eds.; Springer: Dordrecht, The Netherlands, 2006; p 1.
- (47) Donth, E.; Korus, J.; Hempel, E.; Beiner, M. Comparison of DSC Heating Rate and HCS Frequency at the Glass Transition. *Thermochim. Acta* **1997**, *304-305*, 239–249.
- (48) Hensel, A.; Schick, C. Relation Between Freezing-in Due to Linear Cooling and the Dynamic Glass Transition Temperature by Temperature-Modulated DSC. *J. Non-Cryst. Solids* **1998**, *235-237*, 510–510.
- (49) Righetti, M. C. Crystallization of Polymers Investigated by Temperature-Modulated DSC. *Materials* **2017**, *10*, 442.
- (50) Righetti, M. C.; Di Lorenzo, M. L.; Tombari, E.; Angiuli, M. The Low-Temperature Endotherm in Poly(ethylene terephthalate): Partial Melting and Rigid Amorphous Fraction Mobilization. *J. Phys. Chem. B* **2008**, *112*, 4233–4241.
- (51) Wunderlich, B. *Thermal Analysis of Polymeric Materials*; Springer-Verlag: Berlin, 2005; p 689.
- (52) Delpouve, N.; Stoclet, G.; Saiter, A.; Dargent, E.; Marais, S. Water Barrier Properties in Biaxially Drawn Poly(lactic acid) Films. *J. Phys. Chem. B* **2012**, *116*, 4615–4625.
- (53) Billimoria, K.; Heeleyb, E. L.; Parsonsa, N.; Figiela, Ł. An Investigation into the Crystalline Morphology Transitions in Poly-L-lactic acid (PLLA) Under Uniaxial Deformation in the Quasi-Solid-State Regime. *Eur. Polym. J.* **2018**, *101*, 127–139.
- (54) Tadmor, Z. Molecular Orientation in Injection Molding. *J. Appl. Polym. Sci.* **1974**, *18*, 1753–1772.
- (55) Kantz, M. R.; Newman, H. D., Jr.; Stigale, F. H. The Skin-Core Morphology and Structure–Property Relationships in Injection-Molded Polypropylene. *J. Appl. Polym. Sci.* **1972**, *16*, 1249–1260.
- (56) Lu, X. F.; Hay, J. N. Crystallization Orientation and Relaxation in Uniaxially Drawn Poly(ethylene terephthalate). *Polymer* **2001**, *42*, 8055–8067.
- (57) Delpouve, N.; Saiter, A.; Mano, J. F.; Dargent, E. Cooperative Rearranging Region Size in Semi-crystalline Poly(L-lactic acid). *Polymer* **2008**, *49*, 3130–3135.
- (58) Yasuniwa, M.; Sakamo, K.; Ono, Y.; Kawahara, W. Melting Behavior of Poly(L-lactic acid): X-ray and DSC Analyses of the Melting Process. *Polymer* **2008**, *49*, 1943–1951.
- (59) Tábi, T.; Hajba, S.; Kovács, J. C. Effect of Crystalline Forms (α' and α) of Poly(lactic acid) on its Mechanical, Thermo-Mechanical, Heat Deflection and Creep Properties. *Eur. Polym. J.* **2016**, *82*, 232–243.
- (60) Minakov, A. A.; Mordvintsen, D. A.; Schick, C. Melting and reorganization of poly(ethylene terephthalate) on fast heating (1000 K/s). *Polymer* **2004**, *45*, 3755–3763.
- (61) Righetti, M. C.; Gazzano, M.; Di Lorenzo, M. L.; Androsch, R. Enthalpy of melting of α' - and α -crystals of poly(L-lactic acid). *Eur. Polym. J.* **2015**, *70*, 215–220.
- (62) Guinault, A.; Sollogoub, C.; Ducruet, V.; Domenek, S. Impact of Crystallinity of Poly(lactide) on Helium and Oxygen Barrier Properties. *Eur. Polym. J.* **2012**, *48*, 779–788.
- (63) Varol, N.; Delpouve, N.; Araujo, S.; Domenek, S.; Guinault, A.; Golovchak, R.; Ingram, A.; Delbreilh, L.; Dargent, E. Amorphous Rigidification and Cooperativity Drop in Semi Crystalline Plasticized Poly(lactide). *Polymer* **2020**, *194*, 122373.
- (64) Di Lorenzo, M. L.; Righetti, M. C. Effect of Thermal History on the Evolution of Crystal and Amorphous Fractions of Poly[(R)-3-hydroxybutyrate] upon Storage at Ambient Temperature. *Eur. Polym. J.* **2013**, *49*, 510–517.
- (65) Nasser, S. F.; Domenek, S.; Guinault, A.; Stoclet, G.; Delpouve, N.; Sollogoub, C. Structural and Dynamic Heterogeneity in the Amorphous Phase of Poly(L,L-lactide) Confined at the Nanoscale by the Coextrusion Process. *Macromolecules* **2018**, *51*, 128–136.
- (66) Liu, H.; Zhang, J. Research Progress in Toughening Modification of Poly(lactic acid). *J. Polym. Sci., Part B: Polym. Phys.* **2011**, *49*, 1051–1083.
- (67) Lin, J.; Shenogin, S.; Nazarenko, S. Oxygen Solubility and Specific Volume of Rigid Amorphous Fraction in Semicrystalline Poly(ethylene terephthalate). *Polymer* **2002**, *43*, 4733–4743.
- (68) del Rio, J.; Etxeberria, A.; López-Rodríguez, N.; Lizundia, E.; Sarasua, J. R. A PALS Contribution to the Supramolecular Structure of Poly(L-lactide). *Macromolecules* **2010**, *43*, 4698–4707.
- (69) Driesskens, M.; Peeters, R.; Mullen, J.; Franco, D.; Lemstra, P. J.; Hristova-Bogaerds, D. G. Structure versus Properties Relationship of Poly(lactic acid). I. Effect of Crystallinity on Barrier Properties. *J. Polym. Sci., Part B: Polym. Phys.* **2009**, *47*, 2247–2258.
- (70) Fernandes Nassar, S.; Guinault, A.; Delpouve, N.; Divry, V.; Ducruet, V.; Sollogoub, C.; Domenek, S. Multi-scale Analysis of the

Impact of Polylactide Morphology on Gas Carrier Properties. *Polymer* **2017**, *108*, 163–172.

(71) Tashiro, K.; Kobayashi, M. Molecular Theoretical Study of the Intimate Relationship Between Structure and Mechanical Properties of Polymer Crystals. *Polymer* **1996**, *37*, 1775–1786.

(72) Sarge, S. M.; Hemminger, W.; Gmelin, E.; Höhne, G.; Cammenga, H.; Eysel, W. Metrologically Based Procedures for the Temperature, Heat and Heat Flow Rate Calibration of DSC. *J. Therm. Anal.* **1997**, *49*, 1125–1134.

(73) Wurm, A.; Merzlyakov, M.; Schick, C. Reversible Melting Probed by Temperature Modulated Dynamic Mechanical and Calorimetric Measurements. *Colloid Polym. Sci.* **1998**, *276*, 289–296.

(74) Androsch, R.; Moon, I.; Kreitmeier, S.; Wunderlich, B. Determination of Heat Capacity with a Sawtooth-Type, Power Compensated Temperature Modulated DSC. *Thermochim. Acta* **2000**, *357-358*, 267–278.